Journal of Solid State Chemistry 194 (2012) 385–391

Contents lists available at SciVerse ScienceDirect

Journal of Solid State Chemistry

journal homepage: www.elsevier.com/locate/jssc

Synthesis, structure and magnetic properties of $La_3Co_2SbO_9$: A double perovskite with competing antiferromagnetic and ferromagnetic interactions

D.G. Franco [a], V.C. Fuertes [a], M.C. Blanco [a], M.T. Fernández-Díaz [b], R.D. Sánchez [c,*,1], R.E. Carbonio [a,*,1]

[a] INFIQC (CONICET), Departamento de Fisicoquímica, Facultad de Ciencias Químicas, Universidad Nacional de Córdoba, Ciudad Universitaria, X5000HUA Córdoba, Argentina
[b] Institute Laue-Langevin (ILL) 156X, F-38042 Grenoble Cedex 9, France
[c] Centro Atómico Bariloche, CNEA and Instituto Balseiro, Universidad Nacional de Cuyo, Av. Bustillo 9500, 8400 Río Negro, Argentina

ARTICLE INFO

Article history:
Received 7 October 2011
Received in revised form
25 May 2012
Accepted 31 May 2012
Available online 12 June 2012

Keywords:
$La_3Co_2SbO_9$
Double perovskite
Powder neutron diffraction
Rietveld refinement
Ferromagnetic
Magnetic frustration

ABSTRACT

The synthesis, structural characterization, and magnetic properties of $La_3Co_2SbO_9$ double perovskite are reported. The crystal structure has been refined by X-ray and neutron powder diffraction data in the monoclinic space group $P2_1/n$. Co^{2+} and Sb^{5+} have the maximum order allowed for the $La_3Co_2SbO_9$ stoichiometry. Rietveld refinements of powder neutron diffraction data show that at room temperature the cell parameters are $a=5.6274(2)$ Å, $b=5.6842(2)$ Å, $c=7.9748(2)$ Å and $\beta=89.999(3)^\circ$. Magnetization measurements indicate the presence of ferromagnetic correlations with $T_C=55$ K attributed to the exchange interactions for non-linear Co^{2+}–O–Sb^{5+}–O–Co^{2+} paths. The effective magnetic moment obtained experimentally is $\mu_{exp}=4.38\ \mu_B$ (per mol Co^{2+}), between the theoretical one for spin only ($3.87\ \mu_B$) and spin-orbit value ($6.63\ \mu_B$), indicating partially unquenched contribution. The low magnetization value at high magnetic field and low temperature ($1\ \mu_B$/f.u., 5 T and 5 K) and the difference between ZFC and FC magnetization curves (at 5 kOe) indicate that the ferromagnetism do not reach a long range order and that the material has an important magnetic frustration.

1. Introduction

Perovskites and double perovskites in particular are very attractive because of the interest in applications and fundamental areas of advanced materials, catalysis and the many interesting physical properties they have [1].

The general formula of a simple perovskite is ABO_3 and is a highly flexible structure. It can accommodate almost all elements of the periodic table on its cuboctahedral (A) and octahedral (B) sites. The structure of a cubic ideal perovskite can be seen as a three-dimensional array of BO_6 octahedra linked by the vertex, with the A ion in the cuboctahedral cavity surrounded by 8 BO_6 octahedra. Usually an alkali-earth ion occupies the A site [2,3], but a smaller ion, like a lanthanide, can also be accommodated in this site. However, several distortions can arise if the A ion is too small [4]. There are three common distortions: cation displacement within the BO_6 octahedra and distortions and tilting of these octahedra.

When two ions, B and B′, are located on two different crystallographic sites, a double perovskite, $A_2BB'O_6$, is formed. B and B′ ions can be completely or partially ordered among the two different sites. The degree of order depends on the size and charge differences between the B ions. In general, a big difference in size and charge facilitates ordering at the B-site. Nevertheless, other factors, such as specific bonding interactions and synthesis condition may affect the degree of order [5,6]. The magnetic properties are largely affected by the nature of the B cations, for example, B could be a transition metal with unpaired electrons, and if B′ ion has a close shell configuration, then the interactions between B ions and their neighbors will determine the magnetic behavior. Consequently the B order-disorder relationship strongly affects the magnetic properties of these materials [7–9].

In the last years, the synthesis of new double perovskite has resulted in a very attractive topic of research, after it has been informed that Sr_2FeMoO_6 has room temperature colossal magnetoresistance (CMR) [10]. Besides, its half-metallicity, high magnetic transition temperature along with its spin polarized charge transport has a very large importance in the field of spintronics [11] and in applications in read heads, magnetic memories, recording media or field sensors [12].

If the ratio B/B′ in double perovskites is one, the general formula will be $A_2BB'O_6$. For this stoichiometry, in the most ordered case, one of the sites will be fully occupied by B ions, while the other fully occupied by B′. Usually, the formula in this case is written as $A_2(B)(B')O_6$. But if the stoichiometry is $A_3B_2B'O_9$, the maximum order that can be present within B and B′ cations can be written as: $A_2(B)(B_{1/3}B'_{2/3})O_6$ [7], a situation which has an intrinsic disorder, i.e., one of the sites is fully occupied by B but

* Corresponding authors. Fax: +54 351 4334188.
E-mail addresses: rodo@cab.cnea.gov.ar (R.D. Sánchez), carbonio@fcq.unc.edu.ar (R.E. Carbonio).
[1] Members of the Research Career of CONICET.

0022-4596/$ - see front matter © 2012 Elsevier Inc. All rights reserved.
http://dx.doi.org/10.1016/j.jssc.2012.05.045

the other one has a disordered situation, additional disorder could be obtained by moving some B′ to the site fully occupied by B, strongly affecting the magnetic properties [7]. For example, anti-site disorder has been shown to be responsible for spin-glass behavior for different double perovskites, i.e., Sr_2FeTeO_6 [13], $Sr_2Mn_{0.7}Fe_{0.3}O_6$ [14], Sr_2FeMoO_6 [15] among others. The double perovskites $La_3Co_2NbO_9$ and $La_3Co_2TaO_9$ were prepared by our group [16,17] by sol–gel and solid state methods and the correlation between the B order-disorder and magnetic behavior was reported. Samples prepared by solid state showed spontaneous magnetization bellow 72 K for $La_3Co_2TaO_9$ and 62 K for $La_3Co_2NbO_9$ and positive θ values, showing prevalence of ferromagnetic interactions, while those prepared by sol–gel present low spontaneous magnetization (below 40 and 20 K, respectively) and negative θ values, showing prevalence of antiferromagnetic interactions. This behavior was explained by a simple model which shows that the most B-site ordered compounds favors the ferromagnetic Co^{2+}–O–M^{5+}–O–Co^{2+} interactions while the most disordered ones favor the antiferromagnetic Co^{2+}–O–Co^{2+} interactions [16]. These Co^{2+}–O–M^{5+}–O–Co^{2+} ferromagnetic interactions, according to this model, are present in nanoclusters, whose amount and size are highly dependent on the degree of disorder on the B sites.

Here, we describe the synthesis, structure and magnetic characterization of the double perovskite $La_3Co_2SbO_9$, completing in this way the synthesis and characterization of the double perovskites family $La_3B_2B'O_9$ (with B'^{5+} ions) containing Co^{2+} as magnetic ion. $La_3Co_2SbO_9$ was actually informed by the first time by G. Blasse [18] as an orthorhombic perovskite; however no detailed structural or magnetic studies were informed.

2. Experimental

$La_3Co_2SbO_9$ was obtained as reddish-black polycrystalline powder by solid state method. The starting materials, weighed in stoichiometric amounts, were La_2O_3, Co_3O_4 and Sb_2O_3 in analytical grade. The sample was first heat-treated at 950 °C for 12 h, with a second heat treatment, after regrinding, at 1400 °C for 12 h, both in air atmosphere.

Powder X-ray diffraction (PXRD) patterns were measured on a PANalytical X'Pert PRO diffractometer (40 kV, 40 mA) in Bragg–Brentano geometry with Cu K_α radiation (λ=1.5418 Å) at room temperature, between 5° and 120° 2θ in steps of 0.02°. Neutron powder diffraction (NPD) patterns were collected in the D2B powder diffractometer at Institute Laüe-Langevin, Grenoble, France, at room temperature (RT), 150 and 2 K. The measurements were performed between 0° and 160° in 2θ with steps of 0.05°, and the wavelength used was 1.594 Å. Structure refinement of the diffraction patterns were performed by the Rietveld method [19] using the Fullprof program [20]. A pseudo-Voigt shape function was always adequate to obtain good fits for experimental data.

The magnetic characterization was performed in a commercial SQUID magnetometer on powdered samples, between 5 and 300 K, and magnetic fields up to 5 T. The magnetization (M) vs. temperature (T) curves were measured under Zero Field Cooling (ZFC) and Field Cooling (FC) conditions.

3. Results and discussion

3.1. Structural characterization

The PXRD pattern at RT shows a perovskite-like phase with no impurities at all. According to Rietveld refinement result, Fig. 1, $La_3Co_2SbO_9$ crystallizes in a monoclinic structure, space group $P2_1/n$.

Using the following effective ionic radii [21]: rO^{2-}=1.26 Å, $^{XII}(rLa^{3+})$=1.50 Å, $^{VI}(rCo^{2+})$ (HS)=0.885 Å and $^{VI}(rSb^{5+})$=0.74 Å the Goldschmidt tolerance factor (t) calculated for $La_3Co_2SbO_9$ taking into account the partial occupation of the B site by two different cations (Sb^{5+} and Co^{2+} (HS)) is t=0.931, low enough bellow unity to give rise to large deviations from the cubic symmetry. Small shifts in the oxygen positions necessary to accommodate the small La^{3+} ion in the cuboctahedral cavity produce the tilting of the BO_6 octahedra, these tilting generates the reduction in symmetry. These shifts can only be accurately detected by neutrons powder diffraction (NPD) due to the large scattering length of the O nucleus.

The Rietveld fits for the NPD data at RT, 150 and 2 K are displayed in Fig. 2 and also show a good agreement between the calculated and the measured patterns with the space group $P2_1/n$. This space group has two different crystallographic sites for the octahedral ions, Co^{2+} and Sb^{5+}. Anti-site disorder was then refined by assuming Co^{2+} and Sb^{5+} ions can be randomly distributed over these two sites: 2d (½, 0, 0) and 2c (0, ½, 0) Wyckoff positions. The obtained distribution of Co^{2+} and Sb^{5+} was the most possible ordered one for the stoichiometry of the compound, that is the 2d site fully occupied with Co^{2+}, and the 2c site occupied with the remaining Co^{2+} ions and all of the Sb^{5+} ions. Then, the formula of the double perovskite can be written as $La_2(Co)_{2d}(Co_{1/3}Sb_{2/3})_{2c}O_6$. The oxygen occupancies were also refined but they remained close to one within the standard deviations so they were fixed to unity.

Table 1 includes lattice parameters and cell volume, obtained from NPD data refinement at the three temperatures. There is a very small decrease of the cell volume as T decreases. The monoclinic structure obtained shows a β angle very close to 90° for all temperatures, which could show the presence of a tetragonal or orthorhombic symmetry. Because of this situation the tetragonal $I4/m$ and orthorhombic $Immm$ models were also tested. These space groups also allow the order of B and B′ ions as the $P2_1/n$ space group, but show the absence of important Bragg reflections observed in the experimental data, see inset in Fig. 1.

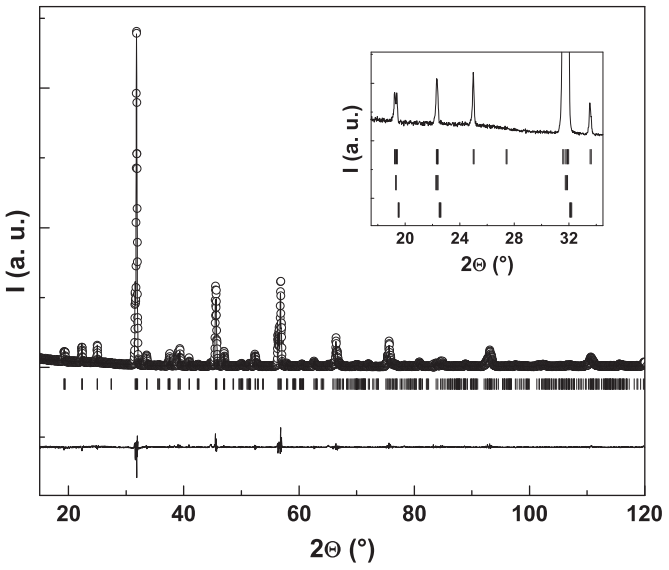

Fig. 1. Rietveld refinement of PXRD data at RT for $La_3Co_2SbO_9$. Observed (circles), calculated (line), and difference (bottom line). Vertical bars represent positions of Bragg reflections for monoclinic double perovskite, space group $P2_1/n$. Reliability factors: χ^2=3.25, R_{wp}=20.1, R_p=17.1, Bragg R-factor=7.70. The inset shows only the experimental data and the Bragg reflections calculated for the space groups $P2_1/n$ (top), $I4/m$ (middle) and $Immm$ (bottom).

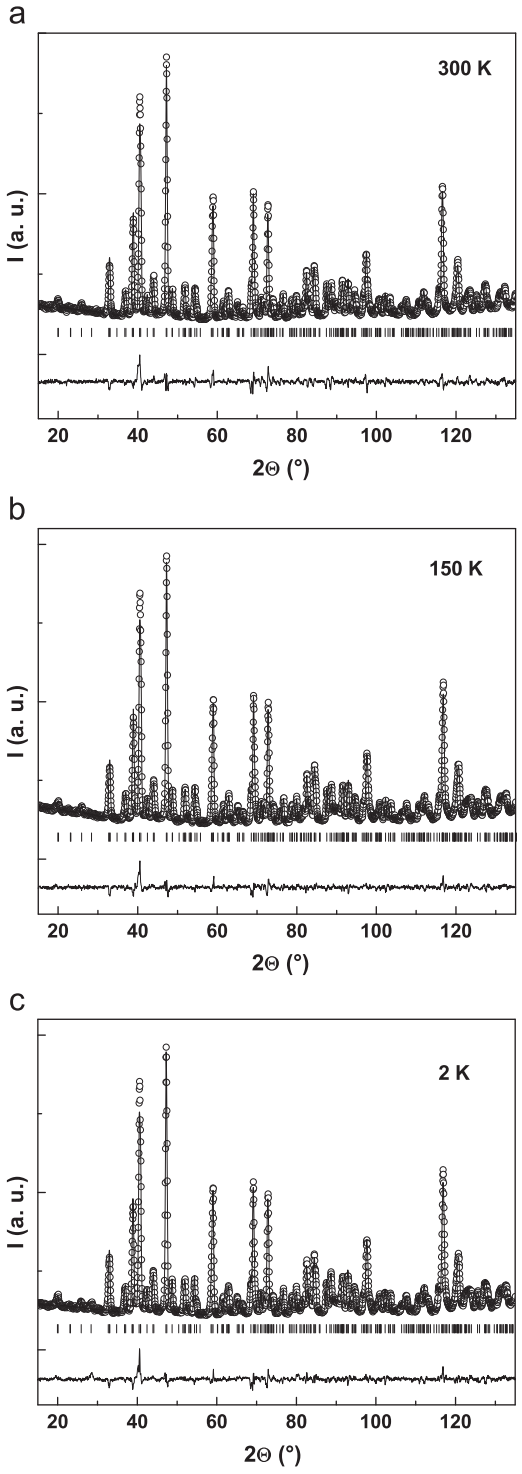

Fig. 2. Rietveld refinement of PND data for $La_3Co_2SbO_9$ taken at 300 K (a), 150 K (b) and 2 K (c) for $La_3Co_2SbO_9$, refined in the $P2_1/n$ space group. Experimental (circles), calculated (line), difference (bottom solid line) and positions of Bragg reflections (vertical bars).

Because of these, we keep the monoclinic structure as the correct one. Table 2 includes Wyckoff sites, final refined atomic coordinates and isotropic thermal factors. Table 3 lists the B–O and B′–O inter-atomic distances and B–O–B′ bond angles and tilt angles for all temperatures. The tilt system for this space group is $a^-a^-c^+$ and the octahedral tilts (δ) are calculated from (Co^{2+})–O–(Co^{2+}/Sb^{5+}) bond angles, as (180°-angle)/2. Fig. 3 shows a polyhedral linkage of the monoclinic double perovskite structure, with the typical rock

Table 1
Lattice parameters and cell volume for $La_3Co_2SbO_9$ at 300, 150 and 2 K, as determined by Rietveld refinements of neutron powder diffraction patterns $\lambda = 1.594$ Å.

T (K)	*a* (Å)	*b* (Å)	*c* (Å)	*β* (°)	Cell volume (Å^3)
300[a]	5.6274(2)	5.6842(2)	7.9748(2)	89.999(3)	255.09(1)
150[b]	5.6196(2)	5.6830(2)	7.9650(2)	90.003(3)	254.4(1)
2[c]	5.6169(2)	5.6838(2)	7.9597(2)	89.997(2)	254.1(1)

Reliable factors:

[a] $\chi^2 = 2.84$; $R_{wp} = 11.1$, $R_p = 11.7$; Bragg R-factor = 4.09.
[b] $\chi^2 = 3.12$; $R_{wp} = 10.1$, $R_p = 10.7$; Bragg R-factor = 4.42.
[c] $\chi^2 = 3.58$; $R_{wp} = 10.5$, $R_p = 11.0$; Bragg R-factor = 3.15.

Table 2
Atomic positions and thermal isotropic factors for $La_3Co_2SbO_9$ at 300, 150 and 2 K as determined from Rietveld refinement of neutron powder diffraction patterns.

Atom	Site	*T* (K)	*x*	*y*	*z*	B_{iso}
La	4e	300	0.4918(3)	0.5391(1)	0.2481(6)	1.40(2)
		150	0.4922(2)	0.5413(1)	0.2491(6)	0.33(1)
		2	0.4914(2)	0.5419(1)	0.2502(6)	1.27(1)
Co	2d	300				0.50(2)
		150	0.5000(0)	0.0000(0)	0.0000(0)	0.10(1)
		2				0.50(2)
Co/Sb	2c	300				0.45(8)
		150	0.0000(0)	0.5000(0)	0.0000(0)	0.76(9)
		2				0.41(7)
O1	4e	300	0.2890(8)	0.2975(6)	0.0387(5)	1.33(8)
		150	0.2896(8)	0.2971(5)	0.0408(6)	1.22(7)
		2	0.2891(7)	0.2979(5)	0.0388(4)	1.19(7)
O2	4e	300	0.2070(7)	0.7845(5)	0.0447(4)	0.40(6)
		150	0.2062(7)	0.7840(5)	0.0440(5)	0.33(5)
		2	0.2050(6)	0.7829(4)	0.0458(4)	0.36(5)
O3	4e	300	0.5799(3)	0.9823(2)	0.2563(6)	1.00(3)
		150	0.5797(2)	0.9824(2)	0.2576(5)	0.83(2)
		2	0.5807(2)	0.9826(2)	0.2572(5)	0.85(2)

Table 3
Bond distances and selected angles for $La_3Co_2SbO_9$ as determined by Rietveld Refinement of neutron powder diffraction at 300, 150 and 2 K.

T (K)	La–O distances (Å)			
300	2.445(5)		2.465(5)	
	2.747(5)		2.840(5)	
	2.759(6)		2.568(1)	
	2.673(5)		2.431(2)	
150	2.444(5)		2.469(5)	
	2.724(5)		2.820(5)	
	2.771(6)		2.555(1)	
	2.674(5)		2.430(2)	
2	2.456(5)		2.455(4)	
	2.719(4)		2.822(5)	
	2.770(5)		2.555(1)	
	2.667(4)		2.428(2)	
T (K)	**Distance (Å)**		**Angle (°)**	**δ(°)**
	Co–O1	Co/Sb–O1	Co–O1–Co/Sb	
	Co–O2	Co/Sb–O2	Co–O2–Co/Sb	
	Co–O3	Co/Sb–O3	Co–O3–Co/Sb	
300	2 × 2.089(4)	2 × 2.016(4)	153.9(2)	13.1
	2 × 2.085(4)	2 × 2.025(3)	153.4(1)	13.3
	2 × 2.095(5)	2 × 1.997(5)	154.0(2)	13.0
150	2 × 2.087(3)	2 × 2.021(4)	153.3(1)	13.4
	2 × 2.087(4)	2 × 2.018(3)	153.6(1)	13.2
	2 × 2.102(4)	2 × 1.985(4)	154.0(1)	13.0
2	2 × 2.090(3)	2 × 2.013(3)	153.7(1)	13.2
	2 × 2.098(3)	2 × 2.010(3)	153.1(1)	13.5
	2 × 2.099(4)	2 × 1.987(4)	153.8(1)	13.1

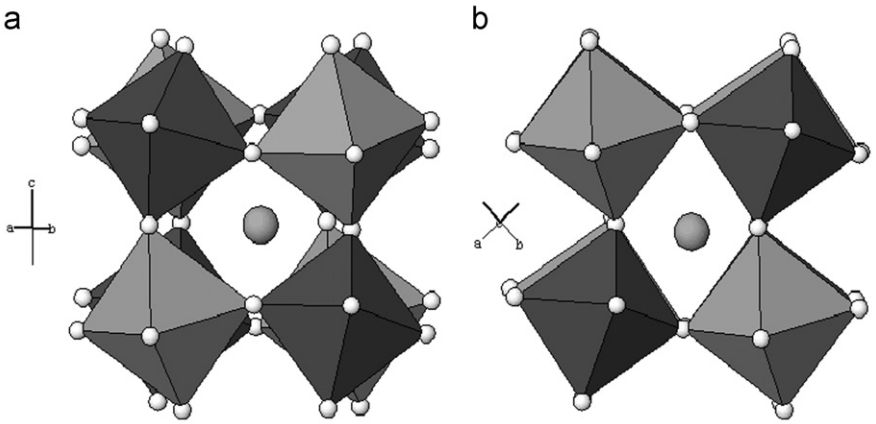

Fig. 3. A polyhedral view of the monoclinic structure of $La_3Co_2SbO_9$ at 300 K showing: the anti-phase (a) and in-phase (b) rotation of the BO_6 and $B'O_6$ octahedra.

Table 4
Bond valence sums for all the ions in $La_3Co_2SbO_9$ at 300, 150 and 2 K, obtained from the Rietveld refinement of neutron powder diffraction data.

Atom	bond valence sums			
	Expected	300 K	150 K	2 K
La	3	2.79(1)	2.82(1)	2.83(1)
Co	2	2.048(9)	2.035(8)	2.02(7)
Co/Sb	2/5	2.52(1)/4.96(2)	2.56(1)/5.03(2)	2.59(1)/5.08(2)
O1	2	1.95(1)	1.95(1)	1.954(9)
O2	2	1.924(9)	1.938(9)	1.962(8)
O3	2	2.013(9)	2.045(8)	2.044(8)

salt arrangement for the octahedral sites. It is noticeable that the bond angles (Co^{2+})–O–(Co^{2+}/Sb^{5+}) are all far from 180°, those in the ideal cubic perovskite structure; this can be assigned to the deviation of the Goldshmidt Tolerance Factor from unity and will be responsible for the peculiar magnetic behavior as will be explained later.

From distances in Table 3 it is noticeable that the octahedron corresponding to 2d site, which only contains Co^{2+} is less distorted that the one containing Co^{2+}/Sb^{5+}. Even thought, the octahedral sites are almost undistorted. The average bond distance of $(Co^{2+}–O^{2-})_{2d}$ bond is 2.090(2) Å while for $(Co^{2+}/Sb^{5+})_{2c}–O^{2-}$ bond is 2.013(2) Å. Both average bond distances are in agreement with those expected from the addition of corresponding ionic radii: 2.15 Å for $Co^{2+}–O^{2-}$ and 2.05 Å for $(Co^{2+}/Sb^{2-})–O^{2-}$ (average value considering stoichiometric relation of both ions), where respective individual ionic radii are for Co^{2+} (HS): 0.885 Å, for Sb^{5+}: 0.74 Å and for O^{2-}: 1.26 Å [21]. The coordination polyhedra for La^{3+} has only 8 distances lower than 3 Å. Taking only this 8 distances, the average bond distance for $La^{3+}–O^{2-}$ is 2.62 Å, which is comparable to the sum (2.56 Å) of ionic radii for $^{VIII}La^{3+}$ (1.3 Å) and O^{2-} (1.26 Å).

Results of the phenomenological Brown's Bond Valence Model [22], can give us and estimation of the actual valences of the cations and anions in the structure. The results are shown in Table 4. There is a very good agreement between these results and the oxidation states of the different ions in the structure. However, it is noticeable that for the 2c site (the site that shares Co^{2+} and Sb^{5+} as a consequence of the intrinsic disorder) has a bond valence sum which is an average of both valence states. This can be explained as a consequence of the existence in the same site of Co^{2+} and Sb^{5+} cations, which causes for Co^{2+} an over estimation in the bond valence sum due to the average short bond distances for its radii and an under estimation for Sb^{5+} due to the larger bond distance calculated for the small Sb^{5+}.

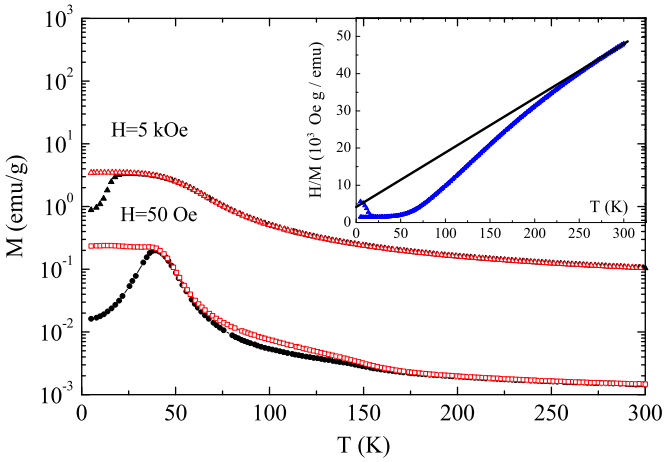

Fig. 4. Magnetization vs. T measured at 50 Oe and 5 kOe. FC: (black), ZFC (red in the online version). The inset shows H/M vs. T and the fit obtained from the Curie–Weiss law at high temperature. (For interpretation of the references to color in this figure legend, the reader is reffered to the web version of this article.)

3.2. Magnetic characterization

The M versus T curves measured at 50 Oe and 5 kOe are displayed in Fig. 4. FC and ZFC curves taken at 50 Oe present a small difference between 175 and 60 K, which is completely well defined below ~40 K, where the ZFC magnetization becomes to decrease towards lower temperatures and the FC branch is practically constant. In general, when FC and ZFC experiments are performed at magnetic fields of thousands of Oe, the difference between both branches disappears. On the contrary, in our system, the ZFC and FC curves at 5 kOe show differences below ~40 K. The ZFC magnetization decreases clearly below ~25 K. These experimental characteristics indicate that the system has some degree of magnetic frustration in the ordered state.

Also, at low temperatures, the M vs. T curve taken after FC shows that the magnetization is practically constant. In frustrated systems made up of magnetic particles, this behavior is an indication of a strong interaction between the particles [23]. In this case, this frustrated system can be considered to be a spin glass or it can be made up of small ferromagnetic cluster interacting between them. Also, around ~55 K in both sets of curves it can be observed an inflection point, which is well defined as the maximum in derivative as a function of temperature (not shown). This point can be considered as the critical magnetic order (T_C~55 K) of $La_3Co_2SbO_9$ independently of the

microscopic model (ferromagnetic cluster glass or spin glass) that can explain the magnetic frustration in this system. In any case, below this T_C temperature, the rapid growth of the magnetization shows the presence of ferromagnetic interactions.

The reciprocal susceptibility (taken as H/M) is linear between 200 and 300 K, the experimental data were fitted with a Curie–Weiss law (H/M=(T-θ)/C) in this temperature range (see inset in Fig. 4), where θ is the Curie–Weiss Temperature and C the Curie constant. The values obtained from the fit are: $\theta=(-10\pm2)$ K and $C=(2.40\pm0.05)$ emu/mol K. The effective magnetic moment obtained from the C parameter is $\mu_{eff}=(4.38\pm0.02)\,\mu_B$/per mol-$Co^{2+}$. The negative sign for θ indicates the presence of antiferromagnetic interactions in the system. For Co^{2+} (HS) with electronic configuration $t_{2g}^5\,eg^2$, the theoretical effective magnetic moment is 3.87 μ_B (spin only) and 6.63 μ_B (spin-orbit). The obtained effective magnetic moment indicates partially unquenched contribution of Co^{2+} in $La_3Co_2SbO_9$, which is usual for Co^{2+} in similar systems [24–29].

The peculiar magnetic behavior in this system is the presence of a ferromagnetic interaction, because in this double perovskite with "intrinsic" B cation disorder, an antiferromagnetic interaction is understandable, since rich patches with Co^{2+}–O–Co^{2+} superexchange interactions are present, like in the antiferromagnetic CoO, but there are other regions rich in Co^{2+}–O–Sb^{5+}–O–Co^{2+} pathways with a p-block diamagnetic ion (Sb^{5+}). Usually, when the angle in this pathway is close to 180°, a weak antiferromagnetic interaction is established because the long range super-super-exchange interaction via B–O–B′–O–B paths. A large list of this class of antiferromagnetic double perovskites with relatively low Néel temperatures can be found in literature [29].

Recently, Retuerto et al. [30,31] have shown that Ca_2CrSbO_6 is one of the few ferromagnetic double perovskites with a B′ diamagnetic ion and they assigned this to the π orbital overlap due to an angle in the pathway Cr^{3+}–O–Sb^{5+}–O–Cr^{3+} which is much lower than 180° (153°). Actually, there is another double perovskite containing Sb^{5+} which is ferrimagnetic, $Sr_3Sb_2NiO_9$ [32], which surprisingly contains two diamagnetic ions (Sb^{5+}) each one paramagnetic (Ni^{2+}), however no detailed fundamental explanation is given in this last case.

In $La_3Co_2SbO_9$, there are simultaneously two magnetic interactions: Co^{2+}–O–Co^{2+} superexchange and Co^{2+}–O–Sb^{5+}–O–Co^{2+} long range super-superexchange. The sign and strength of these couplings depend on the number of d electrons of Co^{2+} ($3d^7$ HS) and the bond angles between Co^{2+}, O^{2-} and Sb^{5+} ions. When the angle between neighboring Co^{2+} is 180° superexchange and super-superexchange are antiferromagnetic (AFM) in nature. Nevertheless, as previously described, Retuerto et al. [30] informed that Ca_2CrSbO_6 shows ferromagnetic (FM) interactions for Cr^{3+}–O–Sb^{5+}–O–Cr^{3+} paths because of the 153° angle between neighboring magnetic ions. This angle is very close to the angle B–O–B′ in $La_3Co_2SbO_9$ (Table 3), which is around 154°. Then, we propose here the appearance of FM interactions for Co^{2+}–O–Sb^{5+}–O–Co^{2+} paths, as observed from the macroscopic magnetic measurements. The coexistence and competition of ferromagnetic and antiferromagnetic interactions can be the origin of the magnetic frustration in this system. The consequence of these two antagonists and microscopic interactions can derivate in two possible ways: one is a spin glass like system where a freezing of the magnetic moments occurs at low temperature, the second possibility can be the formation of small regions with one predominant interaction forming antiferromagnetic and/or ferromagnetic clusters with short range magnetic order. In this last case, cluster-glass like system, we expect at low temperatures the blocking of the magnetic clusters. In order to clarify the more realistic microscopic description of the $La_3Co_2SbO_9$ system, we present hysteresis loops at different temperatures and we study their behavior.

Fig. 5 shows two curves of magnetization versus magnetic field (H) at 5 K. One (black line in the "on-line" version) was after ZFC, while the other (red in the "on-line" version) was after FC conditions. A complex hysteresis loop can be observed composed by a main and irreversible curve in all the measured range, superimposed with an easily magnetizable ferromagnetic component at low fields. The hysteresis loop is shifted around the origin, the corresponding remanent magnetizations are 2.41 and −2.33 emu/g and both coercive fields are very high: 9.05 and −11.31 kOe, respectively. This asymmetry could indicate the presence of exchange bias interactions, which normally occurs in systems where antiferromagnetic and ferromagnetic internal regions are in contact [33–35]. However, we cannot confirm the presence of exchange bias, because the field of the reversibility in a hysteresis loop is not reached by the experimental limit of $H=50$ kOe in our magnetometer. As a consequence, the increasing and decreasing M vs. H curves at high H values go by different ways and the asymmetry can be due to a vertical shift produced by the observation of a "minor loop" as proposed by Geshev [34] and experimentally observed by Yuan et al. [35]. Other interesting point is the saturation magnetization value reached at 50 kOe (~1.5 μ_B/f.u.) by unit formula. This saturation is lower than the expected 2 μ_B/f.u. for the LS and 6 μ_B/f.u. for the HS configuration. This low saturation reached value is another typical characteristic of magnetic frustrated system.

Hysteresis loops between 10 and 50 K are shown in Fig. 6. We observe different kinds of loops depending on the temperature range. At very low temperatures ($T<10$ K), we observe minor loops because our magnetometer is out of range to reach the reversible part of the M vs. H loop at high field. In the middle temperature range we measured normal loops with an important dependence of coercive field with temperature (see Fig. 6a). While, at temperatures between 30 and 50 K approximately (see Fig. 6b) we observe M vs. H curves where the coercive field is practically zero. The loops of this region can scale in a unique curve plotting the M vs. H/T data (solid orange curve). Above these temperatures, we observe a linear M vs. H behavior (not shown here, see the Supplementary Information, Fig. S1: M vs. H at 100 K). The data plotted in Fig. 6b can be described with a Langevin's function with an extra linear component ($M=[a\cdot\coth(bH/T)-(bH/T)^{-1}]+cH/T$) (solid orange curve). The two first terms are due to superparamagnetic behavior which is usually found in magnetic clusters or small particles systems [36]. The last term is a paramagnetic contribution due to isolated and

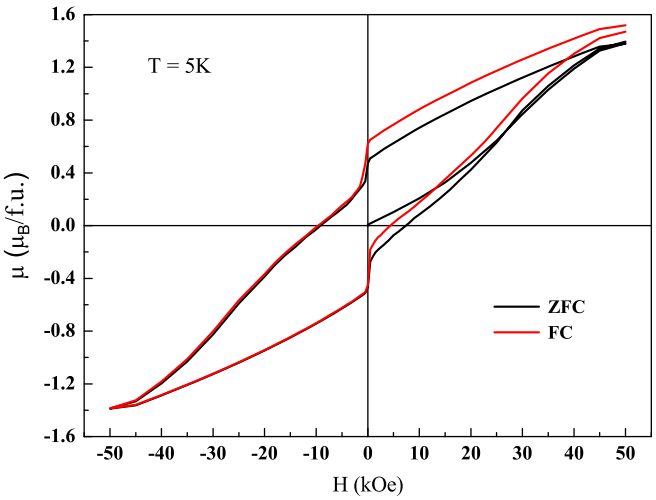

Fig. 5. Hysteresis loop at 5 K taken after ZFC (black "on line") and FC (red "on line") conditions. (For interpretation of the references to color in this figure legend, the reader is reffered to the web version of this article.)

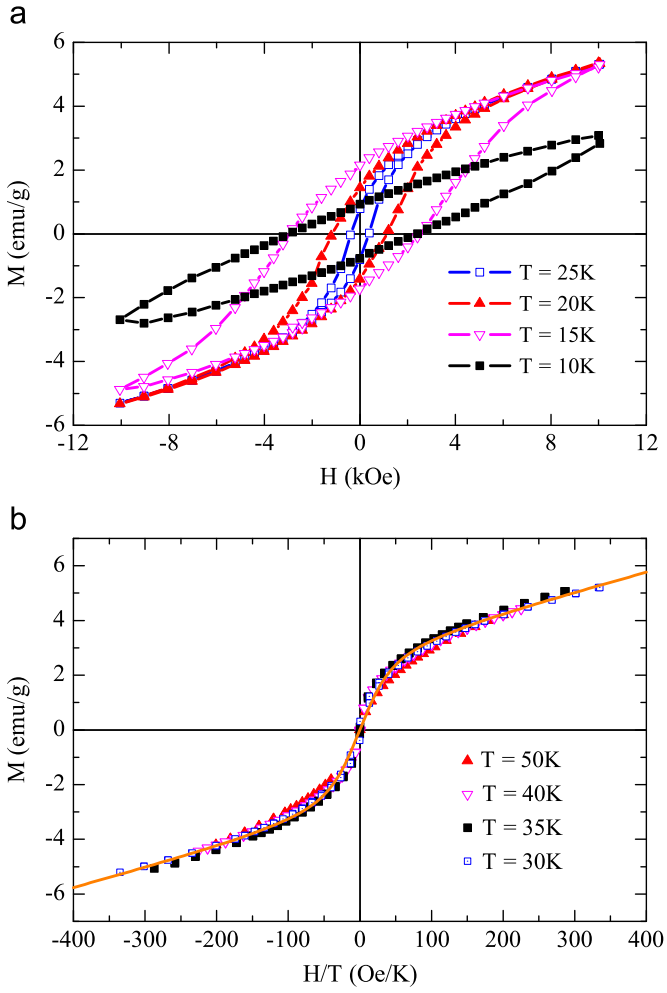

Fig. 6. Hysteresis loop at different temperatures. (a) M vs. H for $T<25$ K and (b) M vs. H/T in the $30<T(\mathrm{K})<50$ temperature range. Solid Curve (orange in the online version) fitted with Langevin's function with an extra linear component $M=[a\cdot\coth(bH/T)-(bH/T)^{-1}]+cH/T$.

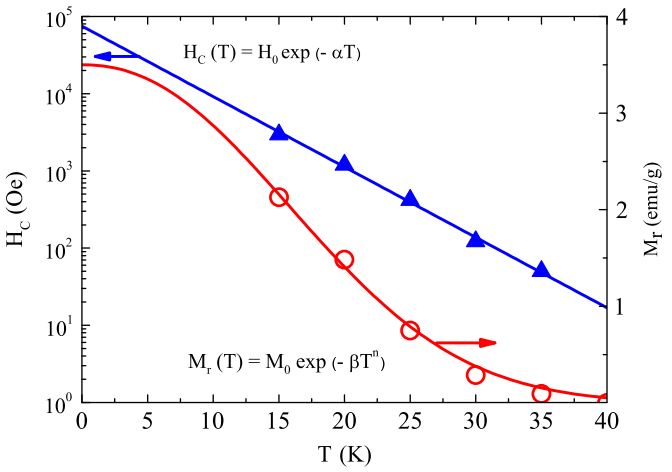

Fig. 7. Log. of the coercive field (Hc) as a function of temperature (left axis). The Hc values is plotted follow a temperature dependence proportional to exp $(-\alpha T)$. On the right axis is the magnetization of remanence as a function of temperature.

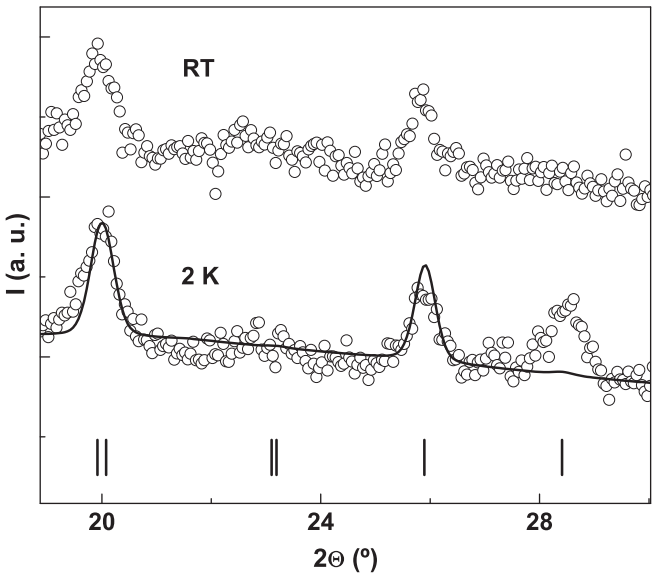

Fig. 8. Detail of the neutron powder diffraction pattern at RT and 2 K, showing the appearance of an extra peak (ca. 28°) due to weak long range magnetic coupling at low temperature. Vertical bars are Bragg positions for the crystallographic cell.

non interacting Co^{2+}. The parameter a is the maximum saturation magnetization (Ms) reached by the clusters ($Ms=3.5$ emu/g) when these are aligned with a high magnetic field; b is a parameter associated with the total magnetic moment of each cluster ($b=\mu/k_B$). We calculate from the fitting that 8% of the cobalt atoms are in clusters with a total magnetic moment around of 620 μ_B/cluster (close to 210 Co^{2+}ions/cluster) and c is the fraction of non-correlated or isolated cobalt ions (approximately 92% of the Co^{2+}ions are free or quasi free).

In Fig. 7 we show the log Hc as a function of temperature (left axis). The linear behavior indicates a H_C $(T)=H^{\circ}_C$ exp $(-\alpha T)$ dependence [37]. The parameters that describe the experimental temperature dependence of the coercivity are $H^{\circ}_C=7.5\times10^4$ Oe and $\alpha=0.21$. Similar behavior is found in systems of the family $La_{1-x}Sr_xCoO_3$ with ferromagnetic short ordering within the clusters [37–39]. This exponential dependence suggests that the blocking of the clusters decreases exponentially with increasing temperature due to thermal activation and α is related to the volume fraction of superparamagnetic particles or nanoclusters [37]. On the right axis of Fig. 7 is plotted the remanence magnetization as a function of temperature in the region where the clusters are blocked. We found a M_r $(T)=M^{\circ}_r$ exp $(-\beta T^n)$ temperature dependence where $n=2.2$, $M^{\circ}_r=3.5$ emu/g and $\beta=1.25\times10^{-3}$. The function is plotted with solid line in the figure. In summary, hysteresis loops show two different behaviors. Below 30 K, coercivity is observed and its temperature dependence is associated with the presence of blocked ferromagnetic clusters, while in the range 55 K $>T>$ 30 K a superparamagnetic behavior is observed due to the non-blocked ferromagnetic clusters.

From 2 K NPD data we can see the appearance of one long range magnetic order reflection at small angle that requires an AFM structure to index it (see Fig. 8). We conclude that this weak magnetic reflection is not enough for the magnetic cell assignment at this stage. Some sort of long range antiferromagnetic order is present at 2 K but there is not enough information to determine the details of this magnetic structure. The long range antiferromagnetic order could be generated on the partial long-range coherence established between antiferromagnetically ordered patches of Co^{2+} spins, composed by some tenths of atoms, naturally arising from the statistical disordering as in the case of Fe^{3+} spins in $Sr_3Fe_2MoO_9$ [40].

The presence of any magnetic impurity like CoO or Co_3O_4 can be discarded, since attempts to refine the magnetic peak using these compounds were unsuccessful (see Supplementary Information, Fig. S2 and S3).

4. Conclusions

The double perovskite $La_3Co_2SbO_9$ was successfully synthesized by solid state method and crystallizes in the monoclinic space group $P2_1/n$, with the highest possible order between Co^{2+} and Sb^{5+} ions and the characteristic intrinsic antisite disorder of the $A_3B_2B'O_9$ stoichiometry. The structure shows tilted octahedra according to $a^-b^-c^+$ system. The small Goldschmidt Tolerance Factor obtained due to the small size of La^{3+}, determines a strong deviation from the ideal cubic symmetry and as a consequence an angle for the path Co^{2+}–O–Sb^{5+}–O–Co^{2+} of 153°, much lower than the one for cubic perovskites, 180°. The named combination of structural features converges in complex magnetic behavior. Magnetization measurements indicate the presence of spontaneous magnetization ($T < 55$ K) attributed to the ferromagnetic exchange interactions for non-linear Co^{2+}–O–Sb^{5+}–O–Co^{2+} paths. The behavior observed of the ZFC and FC magnetization curves is a consequence of disorder of the Sb^{5+} and Co^{2+} ions in the B perovskite sites, which originate a distribution of antiferromagnetic and ferromagnetic interactions between Co neighbors giving a macroscopic magnetic frustrated behavior. Below the temperature where a spontaneous magnetization appears, two different coercivity regions are observed. One of them presents the coercivity with exponential temperature dependence and the second one, with zero coercive field, shows superparamagnetism. Both behaviors can be understood considering the presence of ferromagnetic clusters, which are blocked at low temperatures. These magnetic nanoclusters cannot develop a long range ferromagnetic order giving magnetic frustration.

Supplementary information

Structural information derived from the crystal structure refinement of $La_3Co_2SbO_9$ has been deposited at the ICSD Fachinformationszentrum Karlsruhe (FIZ) (E-mail: CrysDATA@FIZ.Karlsruhe.DE) with ICSD files numbers 423649 (300 K), 423650 (150 K) and 423651 (2 K).

Acknowledgments

R.E.C. thanks ANPCYT (PICT 2007-00303), CONICET and SECYT-UNC for financial support. D.G.F. thanks CONICET for fellowships. R.D.S. thanks ANPCYT (PICT 2011–0752) and Sectyp-UNCu (06/C389). We thank Institut Laue-Langevin (ILL), Grenoble, France for access to D2B line.

Appendix A. Supplementary information

Supplementary data associated with this article can be found in the online version at http://dx.doi.org/10.1016/j.jssc.2012.05.045.

References

[1] R.H. Mitchel, Perovskite Modern and Ancient, Almaz Press, Ontario (2002); Properties and Applications of Perovskite Type Oxides, in: L.G. Tejuca, J.L.G. Fierro (Eds.), Marcel Decker, New York, 1993.
[2] M. Retuerto, M.J. Martínez-Lope, M. García-Hernández, A. Muñoz, M.T. Fernández-Díaz, J.A. Alonso, Mater. Res. Bull. 45 (2010) 1449–1454.
[3] S.A. Ivanov, P. Nordblad, R. Tellgren, A. Hewat, Mater. Res. Bull. 44 (2009) 822–830.
[4] M.W. Lufaso, P.W. Barnes, P.M. Woodward, Acta Crystallogr. B 62 (2006) 397–410.
[5] P.M. Woodward, R.D. Hoffmann, A.W. Sleight, J. Mater. Res. 9 (1994) 2118–2127.
[6] T. Shimada, J. Nakamura, T. Motohashi, H. Yamauchi, M. Karppinen, Chem. Mater. 15 (2003) 4494–4497.
[7] M.C. Viola, M.S. Augsburger, R.M. Pinacca, J.C. Pedregosa, R.E. Carbonio, R.C. Mercader, J. Solid State Chem. 175 (2003) 252–257.
[8] A.S. Ogale, S.B. Ogale, R. Ramesh, T. Venkatesan, Appl. Phys. Lett. 75 (1999) 537–539.
[9] Ll Balcells, J. Navarro, M. Bibes, A. Roig, B. Martínez, J. Fontcuberta, Appl. Phys. Lett. 78 (2001) 781–783.
[10] K.-I. Kobayashi, T. Kimura, H. Sawada, K. Terakura, Nature 395 (1998) 677–680.
[11] M. Bibes, A. Barthelemy, IEEE Trans. Electron. Dev. 54 (2007) 1003–1023.
[12] G.A. Prinz, Science 282 (1999) 1660–1663.
[13] L.O. San Martín, J.P. Chapman, L. Lezama, J.L.S. Garitaonandia, J.S. Macros, J.R. Fernández, M.I. Arriotua, T. Rojo, J. Mater. Chem. 16 (2006) 66–76.
[14] X. Wang, Y. Yu Sui, W. Xu, P. Wang, Liu, J. Tang, J. Appl. Phys. 109 (2011) 07C322.
[15] A. Poddar, R.N. Bhowmik, I.P. Muthuselvam, N. Das, J. Appl. Phys. 106 (2009) 073908–1/8.
[16] V.C. Fuertes, M.C. Blanco, D.G. Franco, J.M. De Paoli, R.D. Sánchez, R.E. Carbonio, Mater. Res. Bull. 46 (2011) 62–69.
[17] V.C. Fuertes, M.C. Blanco, D.G. Franco, J.M. De Paoli, E.V. Pannunzio-Miner, R.D. Sánchez, M.T. Fernández-Díaz, R.E. Carbonio, Physica B 404 (2009) 2717–2719.
[18] G. Blasse, J. Inorg. Nucl. Chem. 27 (1965) 993–1003.
[19] H.M. Rietveld, J. Appl. Crystallogr. 2 (1969) 65–71.
[20] J. Rodríguez-Carvajal, Physica B 192 (1993) 55–69.
[21] R.D. Shannon, Acta Crystallogr. A 32 (1976) 751–757.
[22] I.D. Brown, in: M. O'Keeffe, A. Navrotsky (Eds.), Structure and bonding in crystals, vol. 1, Academic Press, New York, 1981.
[23] C. Papusoi Jr, J. Magn. Magn. Mater. 195 (1999) 708–732, and references there in.
[24] M.C. Viola, M.J. Martínez-Lope, J.A. Alonso, P. Velasco, J.L. Martínez, J.C. Pedregosa, R.E. Carbonio, M.T. Fernández-Díaz, Chem. Mater. 14 (2002) 812–818.
[25] M.C. Viola, M.J. Martínez-Lope, J.A. Alonso, J.L. Martínez, J.M. De Paoli, S. Pagola, J.C. Pedregosa, M.T. Fernández-Díaz, R.E. Carbonio, Chem. Mater. 15 (2003) 1655–1663.
[26] V. Primo-Martin, M. Jansen, J. Solid State Chem. 157 (2001) 76–85.
[27] M.S. Augsburger, M.C. Viola, J.C. Pedregosa, A. Muñoz, J.A. Alonso, R.E. Carbonio, J. Mater. Chem. 15 (2005) 993–1001.
[28] R. Pinacca, M.C. Viola, J.C. Pedregosa, A. Muñoz, J.A. Alonso, J.L. Martínez, R.E. Carbonio, Dalton Trans. (2005) 447–451.
[29] J.W.G. Bos, J.P. Attfield, Phys. Rev. B 70 (2004) 174434.
[30] M. Retuerto, J.A. Alonso, M. García-Hernández, M.J. Martínez-Lope, Solid State Commun. 139 (2006) 19–22.
[31] M. Retuerto, M. García-Hernández, M.J. Martínez-Lope, M.T. Fernández-Díaz, J.P. Attfield, J.A. Alonso, J. Mater. Chem. 17 (2007) 3555–3561.
[32] M. James, J.P. Attfield, J. Rodríguez-Carvajal, J. Phys. Chem. Solids 56 (1995) 1331–1337.
[33] A. Poddar, C. Mazumdar, Mater. Res. Bull. 46 (2011) 682–686.
[34] J. Geshev, J. Magn. Magn. Mater. 320 (2008) 600–602.
[35] S. Yuan, K. Xu, Z. Li, L. Yu, B. Kang, S. Cao, J. Appl. Phys. 105 (2009) 093910.
[36] K. Hayashi, K. Ono, H. Suzuki, M. Sawada, M. Moriya, W. Sakamoto, T. Yogo, Chem. Mater. 22 (2010) 3768–3772.
[37] S. Mukherjee, R. Ranganathan, P. Mondal, J. Phys. Chem. Solids 61 (2000) 1433–1438.
[38] M. Patra, S. Majumdar, S. Giri, J. Phys. Condens. Matter 22 (2010) 116001.
[39] S. Mukherjee, R. Ranganathan, P.S. Anilkumar, P.A. Joy, Phys. Rev. B 54 (1996) 9267–9274.
[40] M.C. Viola, J.A. Alonso, J.C. Pedregosa, R.E. Carbonio, Eur. J. Inorg. Chem. 8 (2005) 1559–1564.